



Design of structures using level set topology optimization and strain energy method

*Bahman Taherkhani**, *Ali Pourkamali Anaraki*, *Javad Kadkhodapour*

Department of Mechanical Engineering, Shahid Rajaee Teacher Training University, Tehran, Iran.

Received: 26 May 2021; Accepted: 12 October 2021

**Corresponding author email: bahman.taherkhani@sru.ac.ir*

ABSTRACT

Level set method (LSM) is a mathematical approach for obtaining structures with specified characterization by moving the interface boundaries between material domain and void domain. This paper used LSM for topology optimization (TO) of a statically loaded structures and also auxetic meta-materials. It is shown that different groups of auxetic structures as very useful materials in many areas, such as the piezoresistive sensor field could be obtained by using level set method. Different groups of auxetic structures obtained by LSM are re-entrant, chiral and some novel auxetic structures that have not been reported before were designed by changing initial design and volume fraction. The scale of production of auxetic structures is in the range of 0.1nm to 10 m and these structures are used in the field of piezoresistive sensors by coating them with ultrafine particles such as nanocarbons. Furthermore, our study revealed that the performance of the code retains the number and direction of symmetries of initial design for final structure. So, auxetic structures with desired symmetries could be designed by using the same symmetries for initial designs.

Keywords: *Level set method (LSM); Auxetic structure; Strain energy based method; Boundary conditions; Shape sensitivity analysis*

1. Introduction

Topology optimization (TO) is a powerful tool which recast the problem as a distribution problem of optimized material in which the system will find the optimized structure in order to satisfy the necessities of goal and constraint functions in an optimization scheme[1]. Approaches based on mathematical algorithms consist of inverse homogenization[2-5], Solid Isotropic Material with Penalization (SIMP)[6-8], Bi-directional Evolutionary structural optimization (BESO) [9, 10] and level set method (LSM)[1, 11-13]. Sigmund[2], who used inverse homogenization theory, firstly represented the application of TO in design of periodic microstructures with prescribed

properties. From that time on, some researchers studied TO method. Sigmund et.al[14] developed a composite materials which have zero or negative thermal expansion coefficient. Sigmund et.al[15] maximized material properties which subject to volume constraint. Torquato et.al[14] represented the design of piezo-composites using TO method. Among the mentioned TO methods, LSM provides great topological flexibility, high shape fidelity, crisp interfaces and smooth boundaries.

LSM[1, 11-13, 16, 17] firstly proposed by Sethian and Osher[18] in 1988 as a method which implicitly represent the evolution of interfaces. In these kind of analysis, the evolution of boundary of interfaces is tracked by solving a so-called Hamilton-jacobi

equation using an appropriate velocity which is normal to the boundary interfaces. In level set approaches, structure boundary is represented by a zero iso-surface of the level set function (LSF) and the value of LSF for points that are in the material domain, void domain and boundary are positive, negative and zero respectively. Sethian Wiegmann[19] used LSM with immersed interface to design structural boundary. Osher and Santosa[11] presented a shape sensitivity analysis using gradient method in order to obtain a velocity field. Allair et.al[20] presented a method in which shape sensitivity analysis is obtained using adjoint variable method. Wang et.al [21] constructed the relation between general structural optimization and LSM through design of calculated velocity field using material derivative in continuum mechanics. Belytschko et.al[22] introduced a method with implicit function and regularization which able to evaluate sensitivity. Wang et.al[23] proposed Radial Bases Functions (RBFs) in order to parameterize LSF and convert the Hamilton-Jacobi equation into a system of ordinary differential equations which not only increased the LSM efficiency but also improved robustness in using multiple constraints.

Auxetic structures are identified by an important property called Poisson's ratio in which Poisson's ratio of these structures are negative [24-28]. In 1987, Lakes[29] produced negative Poisson's ratio Polyurethane foam for the first time and from that time on, researchers[30-38] have interested to study this field more. Auxetic structures have great mechanical properties including shear modulus, fracture toughness, acoustic and vibration absorption. This counterintuitive property caused many applications in different parts of the industry including defense industry, automobile manufacturing, biomedical engineering and sports [34].

The elasticity theory is scale-independent and thus the auxetic structure that is deforming unconventionally might be at a macro scale or micro scale level, or even at the meso scale and molecular levels. As a result, a diversity of negative Poisson's ratio (NPR) structures and materials have been identified, manufactured, or synthesized within the previous years or so, ranging from the macro scale down to molecular levels [39]. Fig.1 shows several number of the artificial and natural NPR materials and structures that now available in the previous studies. Fig.1 also illustrates that composites, polymers, metals and ceramics now exist in NPR form and so we see that NPR structures span all the major types of materials. As we can see, this kind of material and scale range, combined with the new NPR material effect itself and attendant developments in other materials behaviors, means that NPR materials have great capability in a large number of fields, leading to increasing interest of scientists and researchers. One of this fields that auxetic structures made a large improvement in the performance is sensor field. According to Li et al.[40], auxetic sensors with a Poisson's ratio of -0.5 shows a 300% enhancement in sensing performance and the gauge factor boost as much as 500%. To build an auxetic sensor, an auxetic structure, as substrate, is coated with ultrafine materials including nanocarbons, nanotubes and graphene as sensing element.

In this paper, statically loaded structures were designed with maximum stiffness and also 2D NPR (negative Poisson's ratio) structures were obtained by using level-set based TO method. We used strain energy based method to predict the elastic properties of structures (section2). Section3 was about the problem setting for the structure designing. Section4-1 presented illustrative

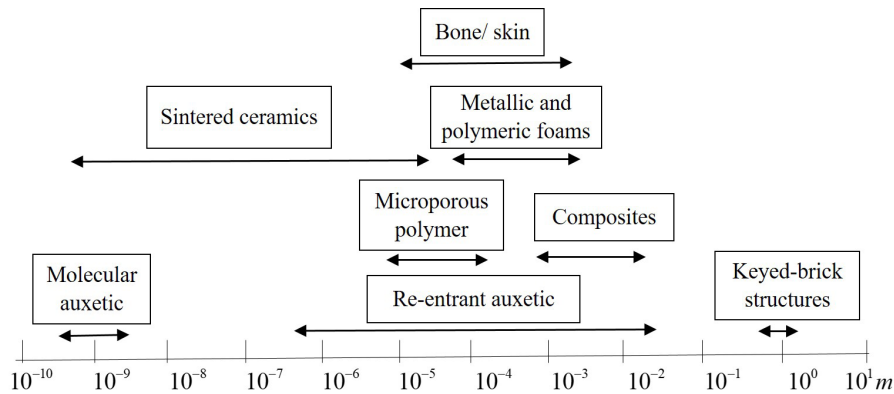


Fig. 1- Length scale of the auxetic structures [39].

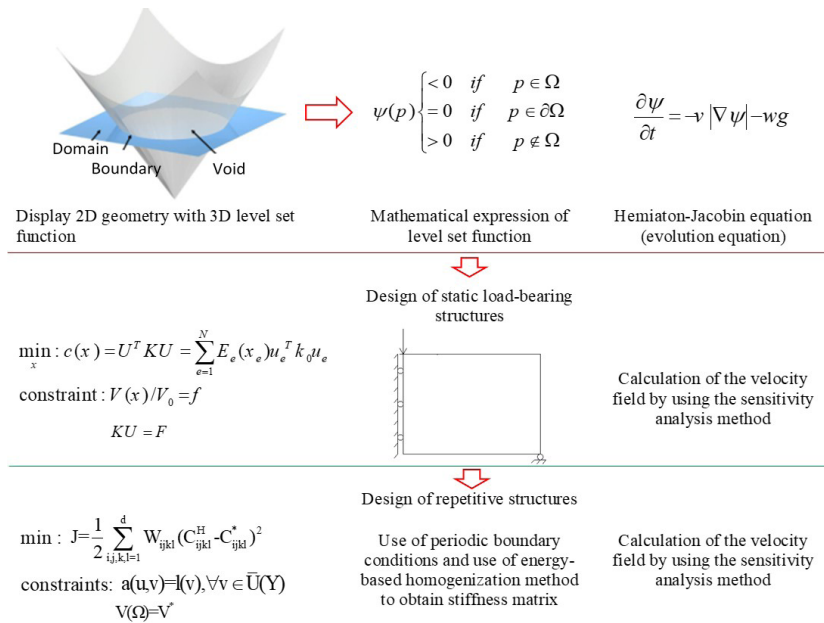


Fig. 2- Schematic view of the level set method for designing load-carrying and NPR structures.

examples including bridge, cantilever and auxetic structures including re-entrant, chiral and some novel auxetic structures. Section4-2 investigated the effects of initial design and volume fraction on final structure. Section4-3 investigated the relation of symmetries between the initial design and final structure and finally Conclusion was provided in section5. Fig.2 shows the level set method for obtaining static load bearing structures and auxetic structures, as well as the relationship between the various parts of this method in the form of the Schematic view. The contents of this figure will be explained in the following sections.

2. Using strain energy method for predicting the elastic properties of the structure unit cell

In this section, the strain energy method was used to determine homogenized elastic tensor [4, 41-44]. In the elastic regime, the relation between effective stress tensor $\bar{\sigma}_{ij}$ and effective strain tensor $\bar{\epsilon}_{kl}$ of anisotropic material unit cell over a homogenized medium was characterized by the following equation:

$$\bar{\sigma}_{ij} = C_{ijkl}^H \bar{\epsilon}_{ij} \tag{1}$$

In which C_{ijkl}^H is called the effective or homogenized elastic tensor which depends upon the volume fraction and the unit cell micro-structure.

In 2D plane stress and for the orthotropic

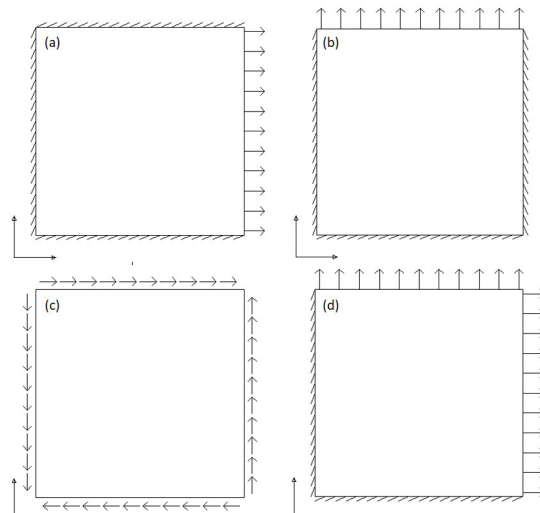


Fig. 3- Displacement boundary conditions for different load cases a) load case 1 for obtaining term of C_{1111} b) load case 2 for obtaining term of C_{2222} c) load case 3 for obtaining term of C_{1122} d) load case 4 for obtaining term of C_{1212} for homogenized stiffness tensor of C.

material, the Eq.1 can be rewritten as follows:

$$\begin{bmatrix} \bar{\sigma}_{11} \\ \bar{\sigma}_{22} \\ \bar{\sigma}_{12} \end{bmatrix} = \begin{bmatrix} C_{1111}^H & C_{1122}^H & 0 \\ C_{1122}^H & C_{2222}^H & 0 \\ 0 & 0 & C_{1212}^H \end{bmatrix} \tag{2}$$

The effective elastic tensor can be obtained with periodicity and boundary condition according to Fig.3 and tab.1. Fig.3 shows the different

Table 1- Strain energy method used to evaluate the efficient elastic tensor for 2D state

case	Strain state	Boundary condition	Strain energy (E^{case})	Terms of C_{ijkl}^H (from eq.2)
1	Horizontal strain ($\bar{\epsilon}_{11}^{(1)} = 1, \bar{\epsilon}_{22}^{(1)} = \bar{\epsilon}_{12}^{(1)} = 0$)	$u_1=1, u_3=0$ $v_2=v_4=0$	$\frac{1}{2} \bar{\sigma}_{11}^{(1)} \bar{\epsilon}_{11}^{(1)} = \frac{1}{2} \bar{\sigma}_{11}^{(1)}$	$C_{1111}^H = 2\bar{E}^{(1)}$
2	Vertical strain ($\bar{\epsilon}_{22}^{(2)} = 1, \bar{\epsilon}_{11}^{(2)} = \bar{\epsilon}_{12}^{(2)} = 0$)	$u_1=u_3=0$ $v_2=1, v_4=0$	$\frac{1}{2} \bar{\sigma}_{22}^{(2)} \bar{\epsilon}_{22}^{(2)} = \frac{1}{2} \bar{\sigma}_{22}^{(2)}$	$C_{2222}^H = 2\bar{E}^{(2)}$
3	Shear strain ($2\bar{\epsilon}_{12}^{(3)} = 1, \bar{\epsilon}_{11}^{(3)} = \bar{\epsilon}_{22}^{(3)} = 0$)	$v_1=u_2=1/4$ $v_3=u_4=-1/4$	$\frac{1}{2} \bar{\sigma}_{12}^{(3)} \bar{\epsilon}_{12}^{(3)} = \frac{1}{2} \bar{\sigma}_{12}^{(3)}$	$C_{1212}^H = 2\bar{E}^{(3)}$
4	Biaxial strain ($\bar{\epsilon}_{12}^{(4)} = 0, \bar{\epsilon}_{11}^{(4)} = \bar{\epsilon}_{22}^{(4)} = 1$)	$u_1=1, u_3=0$ $v_2=1, v_4=0$	$\frac{1}{2} (\bar{\sigma}_{11}^{(4)} \bar{\epsilon}_{11}^{(4)} + \bar{\sigma}_{22}^{(4)} \bar{\epsilon}_{22}^{(4)})$ $= \frac{1}{2} (\bar{\sigma}_{11}^{(4)} + \bar{\sigma}_{22}^{(4)})$	$C_{1122}^H = \bar{E}^{(4)} - \bar{E}^{(1)} - \bar{E}^{(2)}$

boundary conditions used to obtain C_{ijkl}^H and Tab.1 introduces strain energy method to evaluate the terms of efficient elastic tensor. As an illustration, For Fig.3-a, the prescribed horizontal unit strain and displacement boundary conditions are as follows:

$$(\bar{\epsilon}_{11}^{(1)} = 1, \bar{\epsilon}_{22}^{(1)} = \bar{\epsilon}_{12}^{(1)} = 0) \quad (3)$$

$$u_1=1, u_3=0, v_2=v_4=0 \quad (4)$$

The strain energy is:

$$\bar{E}^{(1)} = \frac{1}{2} \bar{\sigma}_{11}^{(1)} \bar{\epsilon}_{11}^{(1)} = \frac{1}{2} \bar{\sigma}_{11}^{(1)} \quad (5)$$

The superscript (1) denotes to the case of loading (Fig.3-a). From Eq.1, we have

$$C_{1111}^H = \bar{\sigma}_{11}^{(1)} / \bar{\epsilon}_{11}^{(1)} = 2\bar{E}^{(1)} \quad (6)$$

The calculation for other cases is similar to this case.

3. TO method algorithm

3.1. Level set method (LSM)

In mathematics, zero level set of a function is a set in which the function takes on the value of zero. LSM, proposed by Sethian and Osher[18], is a computational framework for using level sets as a tool to analysis surfaces and shapes numerically. Following shapes which change topology is easy by using this method. LSF has one more dimension in comparison with level set (iso-surface) and structure boundary is represented implicitly in the zero level set of the LSF.

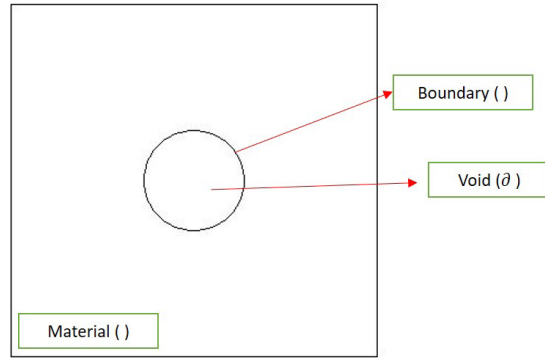


Fig. 4- Iso-surface of a LSF used as an initial design. The domain inside (outside) the hole has negative (positive) value of LSF. The domain on the boundary has zero value of LSF.

Fig.4 demonstrates the LSF ϕ and its intersection with plane xy which creates the structure boundary. Fig.4 illustrates that the domain is divided into three parts in terms of the sign of the LSF:

$$\begin{aligned} \phi(x,t) > 0 & \quad \text{material } (\Omega) \\ \phi(x,t) = 0 & \quad \text{boundary } (\Gamma) \\ \phi(x,t) < 0 & \quad \text{void } (\partial\Omega) \end{aligned} \quad (7)$$

By taking derivative on ϕ in terms of pesedo time t in Eq.7, Hamilton-Jacobi PDE equation can be obtained as follows:

$$\frac{\partial \phi(x,t)}{\partial t} + \nabla \phi(x,t) \cdot V(x) = 0 \quad (8)$$

Which $V(x)=dx/dt$. For normal motion

$$V = V_n n = V_n \frac{\nabla \phi}{|\nabla \phi|} \text{ and } \nabla \phi \cdot \nabla \phi = |\nabla \phi|^2$$

the following equation is obtained from Eq.8:

Table 2- Definition of the parameters of the level set-based TO method

Parameter	Definition
C	Compliance
X	Vector of elements
U	Displacement vector
K	Stiffness matrix
N	Number of elements
x_e	Equal 0 and 1 for void and material elements respectively
k_1	Stiffness matrix for material elements
V(X)	Volume of the structure
V_{req}	Volume fraction constraint
F	Force vector

$$\frac{\partial \phi(x, t)}{\partial t} + V_n |\nabla \phi(x, t)| = 0 \quad (9)$$

Where V_n is velocity field obtaining from shape sensitivity analysis (section3-2).Therefore, the optimization problem is to find a steady-state solution of Eq.9.

3.2. Problem settings

3.2.1. Simple structures

TO problem is the minimization of the mean compliance equation with a single volume constraint as follows[17]:

$$\min_X C(X) = U^T K U = \sum_{e=1}^N u_e^T k_e u_e = \sum_{e=1}^N x_e u_e^T k_1 u_e$$

Subject to: $V(X) = V_{req}$ (10)

$$: KU = F$$

$$: x_e = 0 \text{ or } x_e = 1, \forall e = 1, \dots, N$$

Tab2. Shows parameters definition of Eq.10. Lagrange method was used to combine the volume constraint and the objective function. In order to obtain the parameter of normal velocity (V_n), shape sensitivity analysis was done as follows:

$$C(X) + \lambda^k (V(X) - V_{req}) + \frac{1}{2 \wedge^k} (V(X) - V_{req})^2$$

$$\lambda^{k+1} = \lambda^k + \frac{1}{\wedge^k} (V(X) - V_{req}), \wedge^{k+1} = \alpha \wedge^k \quad (11)$$

λ and \wedge are Lagrange multiplier and k is the iteration number. λ and \wedge are updated in each iteration.

According to Allair et.al [18] and Wang et.al [12, 13] the parameter V_n for statically loaded structure is calculated as follows:

$$\frac{\delta C}{\delta \Omega}_e = -u_e^T k_e u_e$$

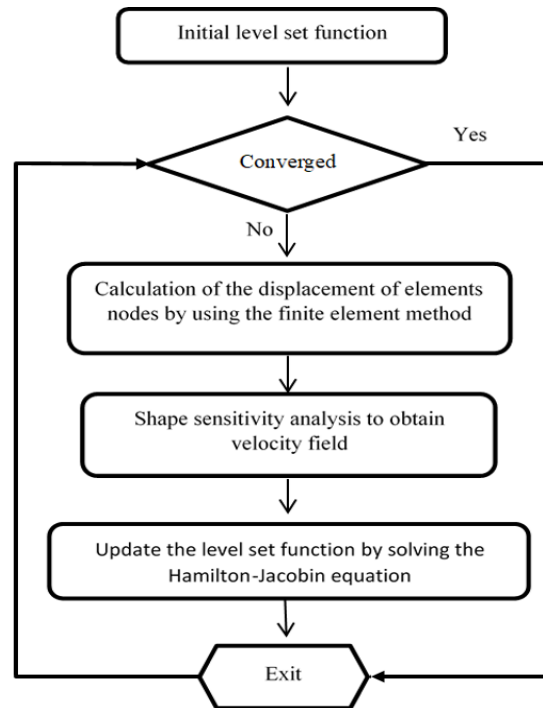


Fig. 5- Design flowchart of load-bearing structures by using level set method.

$$\frac{\delta V}{\delta \Omega}_e = 1 \quad (12)$$

$$V_n|_e = -\frac{\delta L}{\delta \Omega}_e = u_e^T k_e u_e - \lambda^k - \frac{1}{\wedge^k} (V(X) - V_{req})$$

The flowchart of the level set method for the design of load-bearing structures as shown in Fig.5, in which the displacement of the nodes is calculated by the finite element method. The parameter v is calculated by having the displacements and the Hamilton-Jacobin equation is solved by having v, and this procedure continues to satisfy the conditions defined in the constraints and the objective function. In this method, at each

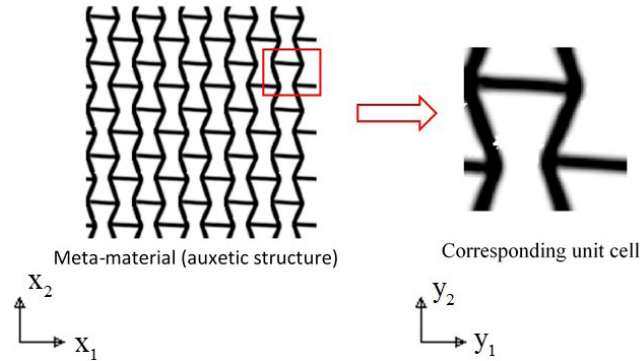


Fig. 6- Meta-materials are created by the juxtaposition of the corresponding unit cells.

iteration, the structure matrix must be converted to a level set function.

3.2.2. Auxetic meta-materials

Metamaterials obtain terrific effective behaviors from rationally designed artificial structures rather than their composition, and so the architecture of the microstructure has an important effect on their behavior as shown in Fig.6. It means that their effective elastic properties depend directly on its microstructure. In this paper, designing mechanical metamaterials with negative Poisson's ratio (NPR), called auxetic structures, is focused. When an auxetic structure is strengthened in the longitudinal direction, it will compact in the transverse direction and vice versa. This contradictory behavior can be used to improve mechanical behavior for the end of increasing the crack resistance, improving the fracture toughness and providing higher sound absorption ability.

In order to design 2D auxetic structures with prescribed effective properties [1, 11, 12, 19], the function J in which the difference between the homogenized material properties C_{ijkl}^H and the prescribed one C_{ijkl}^* must be minimized.

$$J = \frac{1}{2} \sum_{i,j,k,l=1}^d W_{ijkl} (C_{ijkl}^H - C_{ijkl}^*)^2 \quad (13)$$

Where W_{ijkl} is the weighting factor which is dependent on corresponding elasticity tensor and d is related to the design dimension. So, d is 2 for our two dimensional study. There are two constraints consisting of the elasticity equilibrium and volume fraction equations:

$$a(u,v) = l(v), \forall v \in \bar{U}(Y) \quad (14)$$

$$V(\Omega) = V^* \quad (15)$$

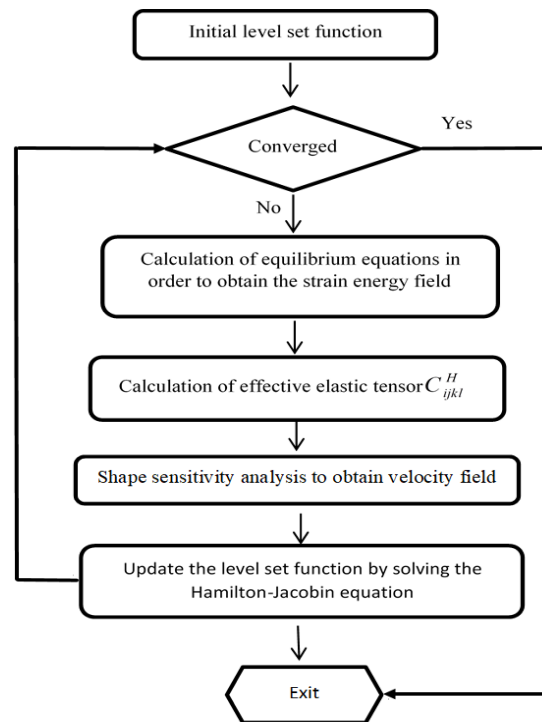


Fig. 7- Flowchart design for repetitive structures by using level set method.

where $a(u,v)$ and $l(v)$ are the bilinear energy form and the linear load form respectively as follows:

$$a(u,v) = \int_D \varepsilon_{ij}^T(u) C_{ijkl} \varepsilon_{kl}(v) H(\phi) d\Omega \quad (16)$$

$$l(v) = \int_D \varepsilon_{ij}^0 C_{ijkl} \varepsilon_{kl}(v) H(\phi) d\Omega \quad (17)$$

$$V(\Omega) = \int_D H(\phi) d\Omega \quad (18)$$

Which $H(\phi)$ is the Heaviside function. In order to minimize the Eq.10, LSF is a regularized sign distance function to prevent too steep or too flat

LSFs. In addition, the Courant-Friedrichs-Lewy (CFL) condition have to be satisfied in order to have numerical stability in solving H-J PDE.

Also, by changing the boundary conditions to periodic boundary conditions and using the strain energy method to obtain an effective stiffness matrix and also changing the objective function and constraints based on part 3-2-1, the flowchart design of structures with negative Poisson's ratio could be obtained according to Fig.7.

4. Results and discussion

4.1. Results

4.1.1. Statically loaded structures

In this part, the proposed optimizer was used to obtain statically loaded structures with different boundary conditions including cantilever and bridge structures. Fig.8 (a) and (b) show the boundary conditions for cantilever and bridge structures, respectively. TO optimizer finds the structure in which the mean compliance of the obtained structures become minimum [8, 16, 17]. Fig.9 shows obtained structures (called cantilever structures) in which their boundary conditions are according to Fig.8 (a). Fig.10 shows obtained structures (called bridge structures) in which their boundary conditions are according to Fig.8 (b).

4.1.2. Grouping of obtained Auxetic structures

In the next section, it will show that different structures could be obtained by changing initial designs and volume fractions. Different group of auxetic structures including re-entrant, chiral and some novel auxetic structures which have not reported in previous works were obtained by changing these two parameters. In this work, we categorized different auxetic structures were obtained by LSM. Fig.11 shows re-entrant auxetic structures [33, 45, 46] that a majority of researchers investigated different aspects of these meta-materials. Fig.12 shows three family of chiral auxetic structures including structures with two

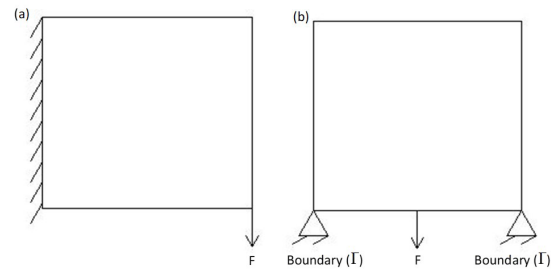


Fig. 8- Boundary condition, force and material domain for (a) cantilever and (b) bridge structures. The optimizer remove some elements of the material domain to obtain the optimized structures.

Volume fraction (%)	Initial design	Final structure
20		
30		
20		
30		

Fig. 9-Volume fraction, initial design and obtained structures for cantilever structures. Different cantilever structures were obtained by using different initial designs and volume fractions.

Volume fraction (%)	Initial design	Final structure
40		
30		
40		
30		

Fig. 10- Volume fraction, initial design and obtained structures for bridge structures. Different bridge structures were obtained by using different initial designs and volume fractions.

Volume fraction (%)	Initial design	Final structure	Poisson's ratio
20			-0.3512
20			-2.164
40			-1.9817
50			-1.8404

Fig. 11- Volume fraction, initial design, final structure and Poisson's ratio for auxetic structures obtained from LSM. Different re-entrant auxetic structures with different values of Poisson's ratios were obtained by using different initial designs and volume fractions.

parts, structures with four parts and rectangular structures. A large number of researchers [5, 24, 30, 47-49] investigated mechanical behavior and deformation pattern of these structures. Fig.13 shows some novel auxetic structures that have not been reported before. These obtained auxetic structures have different Poisson's ratio. So, it would be concluded that the final structure and consequently their Poisson's ratio will be changed by changing the mentioned parameters.

4.2. Discussion

4.2.1. Effects of the initial design and the volume fraction on the final structure

In this part the effect of the initial designs and volume fractions on the final structures were investigated. To this end, two different initial designs and two different volume fractions were considered according to Fig.9. In Fig.9, the initial design in the first and second rows and also for the third and fourth rows are the same and the volume fractions are different and the optimizer finds different final structures for the induced conditions. Similarly, the volume fraction for the rows 1 and 3 and also for the rows 2 and 4 are the same and the initial designs are different and the optimizer finds different final structures too. Therefore, there are two parameters affecting final structures including volume fraction and initial design and the code obtained different final structures by changing each of the mentioned parameters.

There are similar discussion for designing

Structure type	Unite cell	3*3structure	Poisson's ratio	Volume fraction
Two-parts			-0.5742	20%
Two-parts			-0.4667	10%
Four-parts			-1.2295	20%
Four-parts			-0.5466	30%
Novel group			-0.6360	40%
Novel group			-0.6664	40%

Fig. 12- Obtaining different families of chiral auxetic structures including structures with two parts (rows of 1 and 2), structures with four parts (rows of 3 and 4) and structures with rectangular forms (rows of 5 and 6).

bridge structure. The final structures will be changed by changing each of initial designs (compare rows 1 and 3 and also rows 2 and 4) and volume fractions (compare rows 1 and 2 and also rows 3 and 4) according to Fig.10. Similarly for bridge structures, the code obtained different final structures by changing each of the parameters initial designs and volume fractions. It is noticeable that If the initial design is symmetric (non-symmetric), the final structure will be symmetric (non-symmetric) too for both the cantilever and bridge structures as shown in Fig.9 and Fig.10. This issue will be discussed more in the next section.

4.2.2. Axes symmetries

In this section, it was shown that the code will retain the number and direction of symmetry axes of the initial designs in the final structure. To this end, four initial designs with different symmetry axes are solved by the code and the results show that the final structures have the same symmetries (Fig.14). The initial designs of rows 1-4 have 1, 2, 2 and 4 symmetry axes respectively and the same symmetry axes are observable in the final structures. The symmetry axes are shown in red lines. So, auxetic structures with desired symmetries would be obtained by using the same symmetries for initial designs.

Volume fraction (%)	Initial design	Final structure	Poisson's ratio
40			-0.647
40			-0.512
40			-0.4811
50			-0.3471

Fig. 13- Introducing some novel auxetic structures which have not been reported before by using level set topology optimization method.

5. Conclusion

In this paper, LSM for TO of statically loaded structures, including cantilever and bridge structures, and auxetic meta-materials were implemented. Strain energy method was used to obtain effective elasticity matrix in each iteration of solving auxetic meta-material problem. The results showed that final structures (both of statically loaded and auxetic structures) would be different by changing initial design and volume fraction. Furthermore, different categories of auxetic structures including re-entrant, chiral and some novel auxetic structures which have been not reported in previous works were obtained by changing the mentioned parameters. Finally, our study showed that the solver retains the number of axes of initial designs for final structures and it would be possible to obtain final structures with desired symmetries.

References

- Vogiatzis P, Chen S, Wang X, Li T, Wang L. Topology optimization of multi-material negative Poisson's ratio metamaterials using a reconciled level set method. *Computer-Aided Design*. 2017;83:15-32.
- Sigmund O. Materials with prescribed constitutive parameters: An inverse homogenization problem. *International Journal of Solids and Structures*. 1994;31(17):2313-29.
- Hassani B, Hinton E. A review of homogenization and topology optimization I—homogenization theory for media with periodic structure. *Computers & Structures*. 1998;69(6):707-17.
- Bendsøe MP, Kikuchi N. Generating optimal topologies in structural design using a homogenization method.

Initial design	Final structure	Number of symmetry axis
		1
		2
		2
		4

Fig. 14- Initial design with different symmetric axes. The solver retains the number of symmetric axes of initial designs for final structures.

Computer Methods in Applied Mechanics and Engineering. 1988;71(2):197-224.

- Zhang H, Luo Y, Kang Z. Bi-material microstructural design of chiral auxetic metamaterials using topology optimization. *Composite Structures*. 2018;195:232-48.
- Schwerdtfeger J, Wein F, Leugering G, Singer RF, Körner C, Stingl M, et al. Design of Auxetic Structures via Mathematical Optimization. *Advanced Materials*. 2011;23(22-23):2650-4.
- Xia L, Breitkopf P. Design of materials using topology optimization and energy-based homogenization approach in Matlab. *Structural and Multidisciplinary Optimization*. 2015;52(6):1229-41.
- Andreassen E, Clausen A, Schevenels M, Lazarov BS, Sigmund O. Efficient topology optimization in MATLAB using 88 lines of code. *Structural and Multidisciplinary Optimization*. 2011;43(1):1-16.
- He D, Liu S. BESO method for topology optimization of structures with high efficiency of heat dissipation. *International Journal for Simulation and Multidisciplinary Design Optimization*. 2008;2(1):43-8.
- Tang Y, Kurtz A, Zhao YF. Bidirectional Evolutionary Structural Optimization (BESO) based design method for lattice structure to be fabricated by additive manufacturing. *Computer-Aided Design*. 2015;69:91-101.
- Osher SJ, Santosa F. Level Set Methods for Optimization Problems Involving Geometry and Constraints. *Journal of Computational Physics*. 2001;171(1):272-88.
- Wang MY, Wang X. A level-set based variational method for design and optimization of heterogeneous objects. *Computer-Aided Design*. 2005;37(3):321-37.
- Wang Y, Luo Z, Zhang N, Kang Z. Topological shape optimization of microstructural metamaterials using a level set method. *Computational Materials Science*. 2014;87:178-86.
- Sigmund O, Torquato S. Design of materials with extreme thermal expansion using a three-phase topology optimization method. *Journal of the Mechanics and Physics of Solids*. 1997;45(6):1037-67.

15. Gibiansky LV, Sigmund O. Multiphase composites with extremal bulk modulus. *Journal of the Mechanics and Physics of Solids*. 2000;48(3):461-98.
16. Otomori M, Yamada T, Izui K, Nishiwaki S. Matlab code for a level set-based topology optimization method using a reaction diffusion equation. *Structural and Multidisciplinary Optimization*. 2015;51(5):1159-72.
17. Challis VJ. A discrete level-set topology optimization code written in Matlab. *Structural and Multidisciplinary Optimization*. 2010;41(3):453-64.
18. Osher S, Sethian JA. Fronts propagating with curvature-dependent speed: Algorithms based on Hamilton-Jacobi formulations. *Journal of Computational Physics*. 1988;79(1):12-49.
19. Sethian JA, Wiegmann A. Structural Boundary Design via Level Set and Immersed Interface Methods. *Journal of Computational Physics*. 2000;163(2):489-528.
20. Allaire G, Jouve F, Toader A-M. Structural optimization using sensitivity analysis and a level-set method. *Journal of Computational Physics*. 2004;194(1):363-93.
21. Wang MY, Wang X. PDE-Driven Level Sets and Shape Sensitivity for Structural Topology Optimization. Volume 1: 30th Design Automation Conference; 2004/01/01: ASMEDC; 2004.
22. Belytschko T, Xiao SP, Parimi C. Topology optimization with implicit functions and regularization. *International Journal for Numerical Methods in Engineering*. 2003;57(8):1177-96.
23. Wang S, Wang MY. Radial basis functions and level set method for structural topology optimization. *International Journal for Numerical Methods in Engineering*. 2006;65(12):2060-90.
24. Wu W, Song X, Liang J, Xia R, Qian G, Fang D. Mechanical properties of anti-tetrachiral auxetic stents. *Composite Structures*. 2018;185:381-92.
25. Hamzehei R, Kadkhodapour J, Anaraki AP, Rezaei S, Dariushi S, Rezadoust AM. Octagonal auxetic metamaterials with hyperelastic properties for large compressive deformation. *International Journal of Mechanical Sciences*. 2018;145:96-105.
26. Hughes TP, Marmier A, Evans KE. Auxetic frameworks inspired by cubic crystals. *International Journal of Solids and Structures*. 2010;47(11-12):1469-76.
27. Li Y, Luo S, Yang M-C, Liang R, Zeng C. Poisson Ratio and Piezoresistive Sensing: A New Route to High-Performance 3D Flexible and Stretchable Sensors of Multimodal Sensing Capability. *Advanced Functional Materials*. 2016;26(17):2900-8.
28. Saxena KK, Das R, Calius EP. Three Decades of Auxetics Research – Materials with Negative Poisson's Ratio: A Review. *Advanced Engineering Materials*. 2016;18(11):1847-70.
29. Lakes R. Foam Structures with a Negative Poisson's Ratio. *Science*. 1987;235(4792):1038-40.
30. Huang H-H, Wong B-L, Chou Y-C. Design and properties of 3D-printed chiral auxetic metamaterials by reconfigurable connections. *physica status solidi (b)*. 2016;253(8):1557-64.
31. Grima JN, Evans KE. *Journal of Materials Science Letters*. 2000;19(17):1563-5.
32. Hou X, Hu H, Silberschmidt V. A novel concept to develop composite structures with isotropic negative Poisson's ratio: Effects of random inclusions. *Composites Science and Technology*. 2012;72(15):1848-54.
33. Ingrole A, Hao A, Liang R. Design and modeling of auxetic and hybrid honeycomb structures for in-plane property enhancement. *Materials & Design*. 2017;117:72-83.
34. Yang W, Li Z-M, Shi W, Xie B-H, Yang M-B. Review on auxetic materials. *Journal of Materials Science*. 2004;39(10):3269-79.
35. Taherkhani B, Anaraki AP, Kadkhodapour J, Rezaei S, Tu H. Large deformation of TPU re-entrant auxetic structures designed by TO approach. *Journal of Elastomers & Plastics*. 2021;53(4):347-69.
36. Taherkhani B, Azizkhani MB, Kadkhodapour J, Anaraki AP, Rastgordani S. Highly sensitive, piezoresistive, silicone/carbon fiber-based auxetic sensor for low strain values. *Sensors and Actuators A: Physical*. 2020;305:111939.
37. Rezaei S, Kadkhodapour J, Hamzehei R, Taherkhani B, Anaraki AP, Dariushi S. Design and modeling of the 2D auxetic metamaterials with hyperelastic properties using topology optimization approach. *Photonics and Nanostructures - Fundamentals and Applications*. 2021;43:100868.
38. Taherkhani B, Pourkamali Anaraki A, Kadkhodapour J. Fabrication and testing of re-entrant auxetic samples and sensor: Numerically and experimentally. *Amirkabir Journal of Mechanical Engineering*. 2021 Aug 23;53(6 (Special Issue)):14-19.
39. Evans KE, Alderson A. Auxetic Materials: Functional Materials and Structures from Lateral Thinking! *Advanced Materials*. 2000;12(9):617-28.
40. Li Y, Luo S, Yang MC, Liang R, Zeng C. Poisson ratio and piezoresistive sensing: a new route to high-performance 3D flexible and stretchable sensors of multimodal sensing capability. *Advanced Functional Materials*. 2016 May;26(17):2900-8.
41. Zhang W, Dai G, Wang F, Sun S, Bassir H. Using strain energy-based prediction of effective elastic properties in topology optimization of material microstructures. *Acta Mechanica Sinica*. 2007;23(1):77-89.
42. Guedes J, Kikuchi N. Preprocessing and postprocessing for materials based on the homogenization method with adaptive finite element methods. *Computer Methods in Applied Mechanics and Engineering*. 1990;83(2):143-98.
43. Hollister SJ, Kikuchi N. A comparison of homogenization and standard mechanics analyses for periodic porous composites. *Computational Mechanics*. 1992;10(2):73-95.
44. Sigmund O, Maute K. Topology optimization approaches. *Structural and Multidisciplinary Optimization*. 2013;48(6):1031-55.
45. Wang X-T, Li X-W, Ma L. Interlocking assembled 3D auxetic cellular structures. *Materials & Design*. 2016;99:467-76.
46. Zhang ZK, Hu H, Xu BG. An elastic analysis of a honeycomb structure with negative Poisson's ratio. *Smart Materials and Structures*. 2013;22(8):084006.
47. Arredondo JA, Maluendas CR, Valdez F. On the topology of infinite regular and chiral maps. *Discrete Mathematics*. 2017;340(6):1180-6.
48. Prall D, Lakes RS. Properties of a chiral honeycomb with a poisson's ratio of -1 . *International Journal of Mechanical Sciences*. 1997;39(3):305-14.
49. Scarpa F, Blain S, Lew T, Perrott D, Ruzzene M, Yates JR. Elastic buckling of hexagonal chiral cell honeycombs. *Composites Part A: Applied Science and Manufacturing*. 2007;38(2):280-9.